

Thermal post-curing as an efficient strategy to eliminate process parameter sensitivity in the mechanical properties of two-photon polymerized materials

JENS BAUER,¹ ANNA GUELL IZARD,¹ YUNFEI ZHANG,² TOMMASO BALDACCHINI,^{3,4} AND LORENZO VALDEVIT^{1,2,*} 

¹Mechanical and Aerospace Engineering Department, University of California, Irvine, CA 92697, USA

²Materials Science and Engineering Department, University of California, Irvine, CA 92697, USA

³Schmid College of Science and Technology, Chapman University, One University Drive, Orange, CA 92866, USA

⁴Department of Chemistry, University of California, Irvine, CA 92697, USA

*valdevit@uci.edu

Abstract: Two-photon polymerization direct laser writing (TPP-DLW) is one of the most versatile technologies to additively manufacture complex parts with nanoscale resolution. However, the wide range of mechanical properties that results from the chosen combination of multiple process parameters imposes an obstacle to its widespread use. Here we introduce a thermal post-curing route as an effective and simple method to increase the mechanical properties of acrylate-based TPP-DLW-derived parts by 20-250% and to largely eliminate the characteristic coupling of processing parameters, material properties and part functionality. We identify the underlying mechanism of the property enhancement as a self-initiated thermal curing reaction, which robustly facilitates the high property reproducibility that is essential for any application of TPP-DLW.

© 2020 Optical Society of America under the terms of the [OSA Open Access Publishing Agreement](#)

1. Introduction

Two-photon polymerization direct laser writing (TPP-DLW) is one of the most relevant additive manufacturing technologies to synthesize three-dimensional (3D) parts with sub-micrometer resolution [1–3]. TPP locally cures a photosensitive material by simultaneous absorption of two or multiple photons, using a focused ultrafast pulsed laser beam [1]. Polymerization is confined to only the ellipsoid-shaped focal point volume of the laser beam. Dimensions of this volume element, or voxel, can be below 100 nm [1,3], while typical widths and heights are in the range of ≥ 200 nm and ≥ 600 nm, respectively. Most TPP-printed structures are patterned from voxel-lines, i.e. continua of voxels, using galvanometric mirror scanning, 3-axis stage motion, or a combination of both.

The mechanical properties of acrylate-based resins [4,5], the most commonly used TPP materials, are related to the degree of conversion (DC), a measure of the cross-linking density between polymer chains, which is determined by the light exposure dose during printing. The TPP exposure dose, as well as the print quality and speed, mainly correlate with three process parameters: the laser average power (P), the writing speed (v) and the writing density. The latter one can be quantified by the hatching (d_h) and the slicing (d_s) distances between neighboring voxel-lines [6]. Although reaction kinetics differ between resin compositions [7], the fundamental mechanisms governing the mechanical properties are often comparable [8,9], and a similar TPP process parameter dependency may be expected. Several analytical techniques have been established over the years to characterize the DC of photopolymerized materials, including Raman and infrared spectroscopy (the most common) [10,11], and imaging techniques based

on coherent Raman processes [12]. A methodology that holds the promise of distinguishing among thermal, photothermal, and photochemical processes during TPP is the simultaneous use of Raman spectroscopy and differential scanning calorimetry measurements [13].

One obstacle to widespread use of TPP-DLW is the wide range of properties of two-photon-polymerized parts depending on the chosen combination of process parameters [14–17]. While TPP-DLW has been established as a key synthesis route for a broad range of research fields, including photonics [18–20], metamaterials [21–28] and bioscience [29–31], there is no significant industrial application yet. Threshold-based optics models have been shown to well predict the properties of geometrically simple TPP-printed parts as a function of the key process parameters introduced above [14]. However, part-specific variables, like hatching patterns and local feature dimension ranges, in practice compromise property homogeneity, predictability and reproducibility.

Many UV-curing additive manufacturing routes apply post-print processes [32–34], like thermal treatment or UV-flood exposure, to increase and to homogenize cross-linking of as printed, “green” parts; however, neither method is commonly used in TPP. Post-print UV-curing of TPP-parts has been shown inefficient to increase the mechanical properties unless performed in a liquid photoinitiator solution [35]. The impact of thermal post-print treatments on the mechanical properties is not well understood, but beneficial effects on the predictability of the refractive index of several acrylate-based and organic-inorganic hybrid TPP-resins were shown [17].

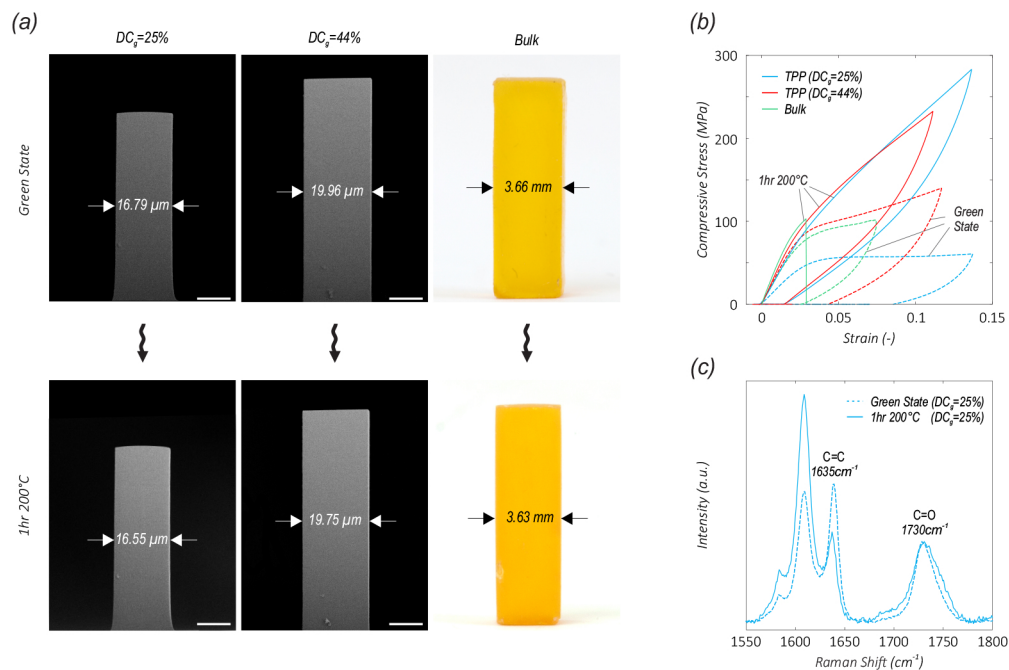


Fig. 1. Thermal post-curing can drastically increase the mechanical properties of two-photon polymerization (TPP) printed resin parts, without affecting shape and surface quality. (a) Multi-voxel-line, hatched TPP specimens and flood exposure cured bulk part from the triacrylate resin IP-Dip, before and after a 1hr vacuum heat treatment at 200°C (scale bars are 10 μm). Representative (b) compressive stress-strain curves and (c) Raman spectra show strength, stiffness, and degree of conversion (DC) increase compared to non-post-cured, green, specimens.

In this paper, we characterize the impact of thermal post-curing on the mechanical properties of the TPP triacrylate resin IP-Dip [36]. Specimens spanned multiple length-scales (Fig. 1(a)), including multi-voxel-line micro-bars as well as bulk samples which were cured by single-photon flood exposure. We measured Young's Modulus (E), yield strength (σ_y) and degree of conversion (DC) by uniaxial compression and Raman micro-spectroscopy, respectively (Figs. 1(b) and (c)). We find that thermal post-curing at 200°C in vacuum can drastically increase the mechanical properties by up to 250%. Increases are highest for the weakest green specimens and gradually decrease to ~20% for green specimens with the highest achievable mechanical properties, thus largely eliminating the characteristic process parameter-property dependencies of TPP-derived parts. Control experiments with only the resin's main monomer pentaerythritol triacrylate (PETA) identify the underlying mechanism of the property enhancement to be a self-initiated thermal curing reaction. The introduced thermal post-curing route is a straightforward method to increase the mechanical properties of TPP-derived parts and to overcome the coupling of process parameters and part properties, robustly facilitating high property reproducibility which is required for any application of TPP-DLW.

2. Materials and methods

2.1. Fabrication

TPP fabrication was carried out with a Photonic Professional GT (Nanoscribe GmbH) DLW system with a Plan-Apochromat 63×1.4 Oil DIC M27 (Carl Zeiss AG) objective and a FemtoFiber pro NIR (TOPTICA Photonics AG) pulsed laser, with a ~100 fs pulse width, a center wavelength of 780 nm, and an 80 MHz repetition rate [37]. The laser average power (P) is the mean power at the objective aperture with a maximum value of 50 mW [37]. The laser beam waist radius (at $1/e^2$) was kept constant throughout all the measurements; specifically, the filling factor was set to 1 so to produce the smallest spot size and minimize power losses. We experimentally measured an objective transmittance of 65%.

TPP specimens from the photoresist IP-Dip (Nanoscribe GmbH, MSDS revision EN01/2017) were printed on fused silica in a layer-by-layer sequence via galvanometric mirror scanning. After TPP-DLW, a 20 min-long propylene glycol monomethyl ether acetate (PGMEA) bath dissolved uncured photoresist, followed by further cleaning in a 5 min-long isopropanol bath. Specimens were then dried in an Autosamdri-931 (Tousimis Research Corp. Inc.) critical point dryer using the automatic mode, whereby the isopropanol bath was exchanged with liquid CO₂ during a single 10 min-long purge cycle followed by a 30 min heating and compression step to the critical point at 31°C and 1350 psi and subsequent cooldown and expansion to ambient conditions. TPP specimens were uniform square-shaped bars with a nominal edge length of 20 μm and a height-to-edge length ratio of 3.25. They were manufactured in a [0/90] laminate manner from unidirectional layers, consisting of multiple voxel-lines with a hatching distance (d_h) and a slicing distance (d_s) between neighboring layers, with a constant hatching-to-slicing-distance ratio ($d_s/d_h=2$). A total of 59 specimens with different combinations of laser average power ($P=9$ -17 mW), writing speed ($v=100$ -8000 μm/s) and writing density ($d_h=0.1$ -0.7 μm) were printed. Within the above ranges, P and d_h were incrementally increased by 0.5 mW and 0.025 μm, and v was increased in steps of 100 μm/s and 1000 μm/s below and above 1000 μm/s, respectively. Two bulk IP-Dip samples with a nominal size of 4 mm x 4 mm x 12 mm were made by 60 min-long single-photon flood exposure in a LQ-Box (Rolence Enterprise Inc.) UV-lamp with 150 mW/cm² average light intensity and a 405 nm peak wavelength. Liquid PETA, the monomer comprising approximately 70% of IP-Dip, was drop cast on fused silica as a control sample [38].

2.2. Experimental characterization

All specimens were heat-treated in a vacuum tube furnace. A heating profile of 3°C/min to 200°C, 60 min hold at 200°C and cooldown to room temperature at 3°C/min was used. Fabrication and characterization protocols were kept consistent and were carried out in a climate-controlled environment, to ensure maximal reproducibility.

Specimen dimensions were measured with a FEI Magellan 400XHR (Thermo Fisher Scientific Inc.) SEM. The density of bulk specimens was determined by weight measurements with a high precision scale and applying the measured dimensions. To determine E and σ_y , we performed uniaxial compression experiments with a strain rate of 0.001sec⁻¹. For TPP specimens, we operated an Alemnis Nanoindenter (Alemnis AG) equipped with a 400 µm-diameter flat punch diamond tip under an optical microscope. Bulk specimens were characterized with the universal test frame Instron 8800 (Instron, ITW Inc.). In both cases, load–displacement curves were recorded. Engineering stress and strain were determined by applying the measured dimensions. E was the maximum slope of the stress-strain curve in the linear elastic regime and σ_y the 0.2% yield offset [39,40].

The DC of TPP specimens and heat-treated PETA was determined via Raman micro-spectroscopy. The confocal Raman microscope inVia (Renishaw plc) was used, with a 50x objective, an excitation wavelength of 785 nm, 50% laser intensity, and 1.5sec - 2sec exposure time, averaged over 15 acquisitions. DC values were extracted as

$$DC = 1 - \left(\frac{A_{C=C}/A_{C=O}}{A'_{C=C}/A'_{C=O}} \right) \quad (1)$$

where $A_{C=C}$ and $A_{C=O}$ are the integrated intensities of carbon-carbon and carbon-oxygen double bond Raman peaks in the polymerized resin, respectively. $A'_{C=C}$ and $A'_{C=O}$ are the integrated intensities of the respective peaks in the unpolymerized resin [10]. The integrated intensities were determined by fitting the corresponding Raman peaks with Lorentzian and Voigt functions [28,35].

3. Results

We examined the impact of a one-hour thermal treatment, at 200°C in vacuum, on the mechanical properties of TPP-printed and single-photon flood exposure cured bulk IP-Dip, as well as the liquid monomer pentaerythritol triacrylate (PETA). E and σ_y of square-shaped TPP-printed and bulk bars were measured by uniaxial compression. For TPP-specimens, the effect of the post-curing treatment was characterized for a wide range of the TPP-parameters, which covered the entire dynamic range of the material, from the solubility to the damage exposure dose threshold. The DC values were calculated from Raman micro-spectroscopy measurements.

Thermal post-curing drastically reduced the pronounced characteristic process-parameter dependencies in the mechanical properties of TPP-derived parts (Fig. 2). Different values of P , v and d_h caused a broad range of degrees of conversion ($DC_g=20-45\%$), yield strengths ($\sigma_g=20-70$ MPa) and Young's moduli ($E_g=0.6-3.6$ GPa) in as-printed, green specimens [14]. By contrast, degree of conversion ($DC_p=68 \pm 4\%$), yield strength ($\sigma_p=81 \pm 3$ MPa) and Young's modulus ($E_p=3.9 \pm 0.4$ GPa) after thermal post-curing were fairly tightly distributed, with only minor process parameter dependency remaining. The treatment thereby drastically increased strength and stiffness of the weakest green specimens by up to 250% and 100%, respectively. Specimens with the highest achievable green properties, printed with TPP-doses approaching the damage threshold of the material, had increased average strength and stiffnesses of 15% and 21%, respectively. Independent from the TPP process-parameter combination, the thermal post-curing treatment did not affect the surface quality and shape of the specimens. Hatching distances of ≥ 0.45 µm resulted in a porous material. For $d_h \geq 0.6$ µm and $v > 6,000$ µm/s, degraded specimen quality prevented mechanical characterization.

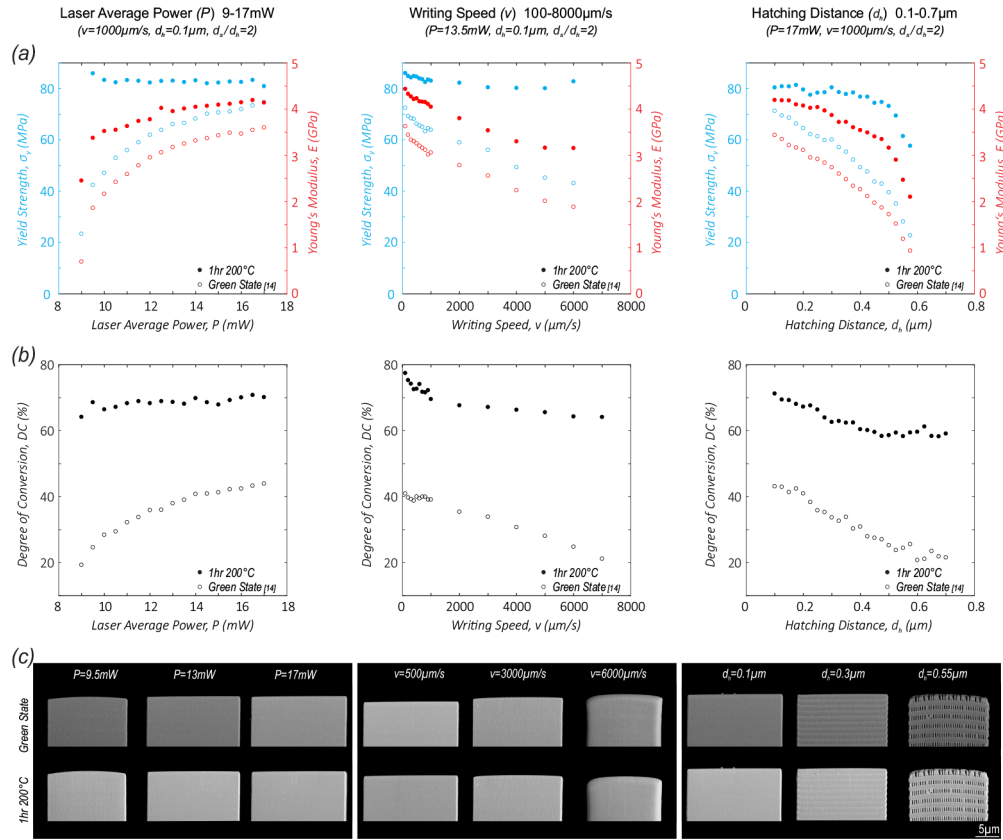


Fig. 2. Thermal post-curing nearly eliminates the characteristic process parameter sensitivity in the mechanical properties of TPP-derived micro-bars. (a) Compressive yield strength (σ_y), blue data points, Young's modulus (E), red data points, and (b) degree of conversion (DC) with and without thermal post-curing, depending on laser average power (P), writing speed (v) and hatching distance (d_h) (left to right column). (c) Close-up SEM images of selected specimens before and after thermal post-curing.

Combining all experimental results from Fig. 2 shows retention of a linear dependency of E_p and σ_p with the green state degree of conversion (DC_g) after thermal post-curing (Fig. 3), albeit with a notably reduced process parameter dependency and overall increased properties compared to the green strength (σ_g) and stiffness (E_g). As for the green state, post-cured specimens with the same green state degree of conversion roughly have the same mechanical properties, independent from specific process parameters. Notably, the strength is thereby almost independent on DC_g , whereas the stiffness and the degree of conversion (DC_p) retain a notable dependency on DC_g (Figs. 3(a)–(c)). σ_p , E_p and DC_p approximately correlate with DC_g as:

$$\sigma_p = (29.5DC_g + 70.5) \text{ MPa} \quad (2)$$

$$E_p = (5.87DC_g + 1.76) \text{ GPa} \quad (3)$$

$$DC_p = (0.55DC_g + 0.48) \quad (4)$$

Figure 3(d) compares the degree of conversion gain (ΔDC) of the TPP-specimens by thermal post-curing, given by $\Delta DC = DC_p - DC_g$, to the DC of pentaerythritol triacrylate (PETA), the monomer comprising approximately 70% of IP-Dip, [38] after identical thermal treatment. Liquid

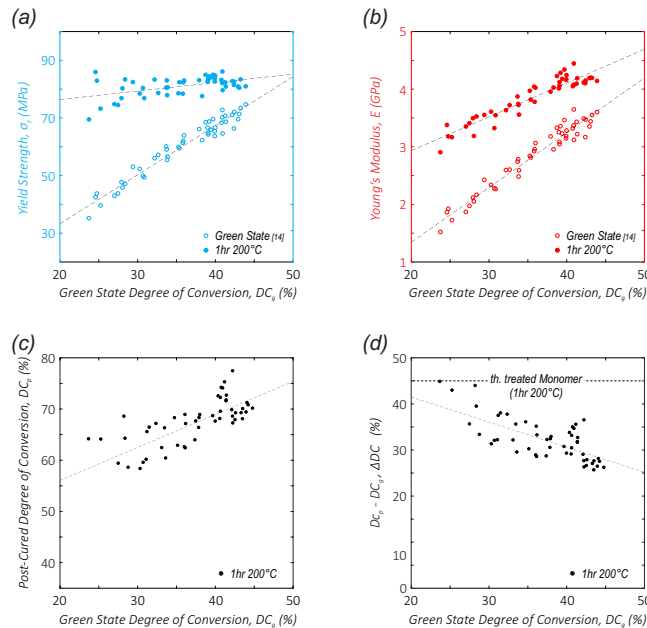


Fig. 3. Combining the data of all specimens from Fig. 2 shows thermal post-curing notably increases the mechanical properties of TPP-derived hatched multi-voxel-line specimens, while retaining linear scaling with the green state degree of conversion (DC_g), independent from specific process parameters. (a) Compressive yield strength (σ_y), (b) Young's modulus (E) and (c) degree of conversion (DC) with and without thermal treatment, and (d) degree of conversion increase upon thermal post-curing (ΔDC); the dotted line in (d) indicates the DC of PETA, the monomer constituting $\sim 70\%$ of IP-Dip, after the same thermal treatment as applied to the TPP-specimens.

PETA was drop cast onto a fused silica slide and subjected to a one-hour thermal treatment at 200°C in vacuum. While PETA does not contain any initiator, the treatment caused it to solidify and to cross-link with a DC of $45.1 \pm 0.2\%$. This DC value agrees well with the highest degree of conversion gains that we measured upon post-curing, which were exhibited by the TPP-specimens with the lowest achievable green properties.

Thermal post-curing increased the mechanical properties of single-photon flood exposed bulk specimens in a similar way as for TPP-derived parts. After one-hour at 200°C in vacuum, yield strength and Young's Moduli of bulk specimens, with nominal dimension of $0.4 \times 0.4 \times 1.2$ cm, increased from 62 ± 5 MPa to 81 ± 1 MPa and from 3.1 ± 0.2 GPa to 4.3 ± 0.4 GPa, respectively. As for the green state, [14] the bulk post-cured properties correspond to those of TPP-specimens with DC_g in the range of 35-40%. Compared to the green state, the density of bulks specimens increased by $\sim 2\%$ to 1.27 ± 0.01 g/cm³, which correlates with the observed slight linear shrinkage.

Figure 4 shows the linear shrinkage of multi-voxel-line micro-bars depending on their green state degree of conversion before and after thermal post-curing at 200°C . The shrinkage is calculated as the ratio of SEM measured dimensions and the nominal dimensions of $20 \times 20 \times 65$ μm . The shrinkage of as-printed, green, specimens strongly depends on DC_g [14,41], while the minor additional linear shrinkage of $1.2 \pm 0.4\%$, upon thermal post-curing, is independent of the green state properties.

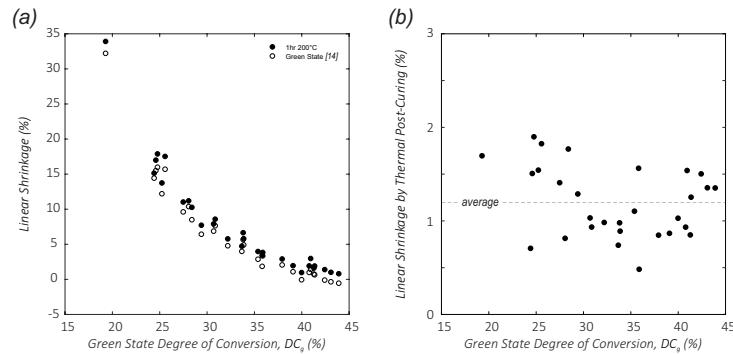


Fig. 4. Linear shrinkage of green state and thermally post-cured TPP-derived micro-bars, with respect to the nominal dimensions, depending on the green state degree of conversion (DC_g); (a) Absolute values and (b) contribution of the thermal treatment. The shown data comprises all specimens of Fig. 2.

4. Discussion

During the UV-curing of acrylate-based resins, polymerization is initiated via the absorption of photons by photoinitiator molecules, which then cleave into primary radicals starting a polymerization reaction that proceeds by a radical chain growth mechanism [42]. Thereby, the polymerization process under the experimental conditions employed in this work is photo-chemical, given that the temperature rise at the laser focal spot upon writing is minimal [43]. The degree of conversion and hence the mechanical properties are proportional to the density of radicals (ρ) which are generated. In TPP, ρ can strongly vary depending on the exposure dose distributions for given processing conditions. Steric hindrance and decreased diffusion eventually cause “trapping” of active species in the solidifying polymer, complicating further cross-linking and limiting the maximum mechanical properties [44,45].

Post-print UV-curing of TPP-derived parts can only marginally increase cross-linking unless additional photoinitiator molecules from an external source infiltrate the material, for example when parts are submerged in a photoinitiator solution during UV-flood exposure [35]. This approach has successfully been applied to open-cell lattice structures with nanometer-size features. However, many applications include notably larger features, for which the longer diffusion paths may be expected to decrease the efficiency of the process.

Thermal post-curing of acrylate based-resins is achieved via thermal self-initiation reactions, which do not depend on an initiator diffusing inwards and hence are not part-geometry sensitive. At temperatures above 120°C, acrylic monomers and oligomers can polymerize in absence of any known thermal initiator [46–48]. Computational quantum chemistry studies have shown that monoradicals thereby form via hydrogen transfer or abstraction, initiating chain scission and intramolecular chain transfer [48]. Our control experiments with initiator-free PETA (Fig. 3(d)) indicate that such self-initiation mechanisms are the key contributors to increased cross-linking and mechanical properties of both TPP-printed specimens and single-photon flood exposed bulk parts via thermal post-curing. The observed increasing effect of the treatment with decreasing green properties suggests that the efficiencies of the thermally self-initiated chain scission and transfer are dependent on the green state degree of conversion, with the higher chain mobility and flexibility of minimally pre-cross-linked specimens being favorable. In addition to self-initiation, the elevated temperature increases the mobility of trapped photo-initiated radicals, accelerating reactions which were at room temperature halted by steric hindrance [17]. All thermally induced polymerization reactions are expected to be temperature dependent; thus, higher post-curing temperatures than investigated in this study could allow further property increases and potentially

complete independence from process parameters. The caveat is that for temperatures well above 200°C onset of decomposition may eventually reduce properties again, suggesting the existence of an optimal post-curing temperature [49].

5. Conclusion

Here we have introduced a thermal post-curing route as an effective and simple method to notably enhance cross-linking and mechanical properties of TPP-derived parts, and to partially erase their pronounced process parameters dependency. Different process parameter combinations, and even printing patterns and part geometries, have been shown to entail a wide range of mechanical properties for two-photon-polymerized materials [14]. While this may be considered a great potential from a material design point of view, it poses significant challenges to property reproducibility and reliability, which are key in any applications, specifically ones driven by industrial interests. The findings of this study provide a pathway to overcoming these crucial limitations, thus enabling more widespread use of TPP-DLW. Future studies will concentrate on calorimetric measurements of TPP-derived parts to interpret thermal post-processing mechanisms at the molecular level.

Beyond its impact on mechanical behavior, thermal post-curing is an effective method to increase other properties including optical characteristics like the refractive index [17]. Unlike in UV-post curing in a photoinitiator solution, the efficiency of thermal post-curing may be independent of the part geometry and size [35]. The findings of this study are expected to transfer to different acrylate-based and other resin systems.

Funding

Air Force Office of Scientific Research (FA9550-14-1-0352); National Science Foundation (CMMI-1905582); Deutsche Forschungsgemeinschaft (BA 5778/1-1).

Acknowledgements

J.B., T.B. and L.V. conceived the research, J.B., A.G. and Y.Z. manufactured specimens and performed mechanical experiments, J.B. performed Raman measurements, J.B. and A.G. analyzed data, J.B., T.B. and L.V. interpreted results, and J.B. wrote the manuscript. SEM imaging was conducted at the UCI Materials Research Institute (IMRI). Raman measurements were conducted at the UCI Laser Spectroscopy Lab. The authors are thankful to Dimitry Fishman for useful discussions on Raman spectroscopy.

Disclosures

The authors declare no conflicts of interest.

References

1. T. Baldacchini, *Three-Dimensional Microfabrication Using Two-Photon Polymerization*, 1st ed. (Elsevier, 2015).
2. K.-S. Lee, R. H. Kim, D.-Y. Yang, and S. H. Park, "Advances in 3D nano/microfabrication using two-photon initiated polymerization," *Prog. Polym. Sci.* **33**(6), 631–681 (2008).
3. J. K. Hohmann, M. Renner, E. H. Waller, and G. von Freymann, "Three-Dimensional μ -Printing: An Enabling Technology," *Adv. Opt. Mater.* **3**(11), 1488–1507 (2015).
4. L. H. Nguyen, M. Straub, and M. Gu, "Acrylate-Based Photopolymer for Two-Photon Microfabrication and Photonic Applications," *Adv. Funct. Mater.* **15**(2), 209–216 (2005).
5. T. Baldacchini, C. N. Lafratta, R. A. Farrer, M. C. Teich, B. E. A. Saleh, M. J. Naughton, and J. T. Fourkas, "Acrylic-based resin with favorable properties for three-dimensional two-photon polymerization," *J. Appl. Phys.* **95**(11), 6072–6076 (2004).
6. T. Bormann, B. Müller, M. Schinhammer, A. Kessler, P. Thalmann, and M. de Wild, "Microstructure of selective laser melted nickel–titanium," *Mater. Charact.* **94**, 189–202 (2014).
7. E. Waller, G. von Freymann, E. H. Waller, and G. von Freymann, "Spatio-Temporal Proximity Characteristics in 3D μ -Printing via Multi-Photon Absorption," *Polymers* **8**(8), 297 (2016).

8. J. Serbin, A. Egbert, A. Ostendorf, B. N. Chichkov, R. Houbertz, G. Domann, J. Schulz, C. Cronauer, L. Fröhlich, and M. Popall, "Femtosecond laser-induced two-photon polymerization of inorganic–organic hybrid materials for applications in photonics," *Opt. Lett.* **28**(5), 301 (2003).
9. S. Shukla, X. Vidal, E. P. Furlani, M. T. Swihart, K.-T. Kim, Y.-K. Yoon, A. Urbas, and P. N. Prasad, "Sub-wavelength Direct Laser Patterning of Conductive Gold Nanostructures by Simultaneous Photopolymerization and Photoreduction," *ACS Nano* **5**(3), 1947–1957 (2011).
10. L. J. Jiang, Y. S. Zhou, W. Xiong, Y. Gao, X. Huang, L. Jiang, T. Baldacchini, J.-F. Silvain, and Y. F. Lu, "Two-photon polymerization: investigation of chemical and mechanical properties of resins using Raman microspectroscopy," *Opt. Lett.* **39**(10), 3034–3037 (2014).
11. K. Cicha, Z. Li, K. Stadlmann, A. Ovsianikov, R. Markut-Kohl, R. Liska, and J. Stampfl, "Evaluation of 3D structures fabricated with two-photon-photopolymerization by using FTIR spectroscopy," *J. Appl. Phys.* **110**(6), 064911 (2011).
12. T. Baldacchini, M. Zimmerley, C.-H. Kuo, E. O. Potma, and R. Zadayan, "Characterization of Microstructures Fabricated by Two-Photon Polymerization Using Coherent Anti-Stokes Raman Scattering Microscopy," *J. Phys. Chem. B* **113**(38), 12663–12668 (2009).
13. T. Suzuki, J. Morikawa, T. Hashimoto, R. Buividas, G. Gervinskas, D. Paipulas, M. Malinauskas, V. Mizeikis, and S. Juodkazis, "Thermal and optical properties of sol-gel and SU-8 resists," in *Advanced Fabrication Technologies for Micro/Nano Optics and Photonics V*, W. V. Schoenfeld, R. C. Rumpf, and G. von Freymann, eds. (SPIE, 2012), 8249, p. 82490 K.
14. J. Bauer, A. Guell Izard, Y. Zhang, T. Baldacchini, and L. Valdevit, "Programmable Mechanical Properties of Two-Photon Polymerized Materials: From Nanowires to Bulk," *Adv. Mater. Technol.* **4**(9), 1900146 (2019).
15. T. Baldacchini, C. N. LaFratta, and M. Malinauskas, "Metrology and process control," in *Three-Dimensional Microfabrication Using Two-Photon Polymerization* (Elsevier, 2020) pp. 197–228.
16. A. Butkutė, L. Čkanavičius, G. Rimšelis, D. Gailevičius, V. Mizeikis, A. Melninkaitis, T. Baldacchini, L. Jonušauskas, and M. Malinauskas, "Optical damage thresholds of microstructures made by laser three-dimensional nanolithography," *Opt. Lett.* **45**(1), 13 (2020).
17. M. Schmid, D. Ludescher, and H. Giessen, "Optical properties of photoresists for femtosecond 3D printing: refractive index, extinction, luminescence-dose dependence, aging, heat treatment and comparison between 1-photon and 2-photon exposure," *Opt. Mater. Express* **9**(12), 4564 (2019).
18. N. Lindenmann, G. Balthasar, D. Hillerkuss, R. Schmogrow, M. Jordan, J. Leuthold, W. Freude, and C. Koos, "Photonic wire bonding: a novel concept for chip-scale interconnects," *Opt. Express* **18**(17), 1290–1292 (2011).
19. M. Schumann, T. Bückmann, N. Gruhler, M. Wegener, and W. Pernice, "Hybrid 2D–3D optical devices for integrated optics by direct laser writing," *Light: Sci. Appl.* **3**(6), e175 (2014).
20. L. Jonušauskas, D. Gailevičius, S. Reškštytė, T. Baldacchini, S. Juodkazis, and M. Malinauskas, "Mesoscale laser 3D printing," *Opt. Express* **27**(11), 15205 (2019).
21. C. M. Soukoulis and M. Wegener, "Past achievements and future challenges in the development of three-dimensional photonic metamaterials," *Nat. Photonics* **5**(9), 523–530 (2011).
22. G. von Freymann, A. Ledermann, M. Thiel, I. Staude, S. Essig, K. Busch, and M. Wegener, "Three-Dimensional Nanostructures for Photonics," *Adv. Funct. Mater.* **20**(7), 1038–1052 (2010).
23. J. Bauer, L. R. Meza, T. A. Schaedler, R. Schwaiger, X. Zheng, and L. Valdevit, "Nanolattices: An Emerging Class of Mechanical Metamaterials," *Adv. Mater.* **29**(40), 1701850 (2017).
24. J. Bauer, A. Schroer, R. Schwaiger, and O. Kraft, "Approaching theoretical strength in glassy carbon nanolattices," *Nat. Mater.* **15**(4), 438–443 (2016).
25. J. Bauer, S. Hengsbach, I. Tesari, R. Schwaiger, and O. Kraft, "High-strength cellular ceramic composites with 3D microarchitecture," *Proc. Natl. Acad. Sci. U. S. A.* **111**(7), 2453–2458 (2014).
26. J. Bauer, C. Crook, A. Guell Izard, Z. C. Eckel, N. Ruvalcaba, T. A. Schaedler, and L. Valdevit, "Additive Manufacturing of Ductile, Ultrastrong Polymer-Derived Nanoceramics," *Matter* **1**(6), 1547–1556 (2019).
27. C. Crook, J. Bauer, A. Guell Izard, C. Santos de Oliveira, J. Martins de Souza e Silva, J. B. Berger, and L. Valdevit, "Plate-nanolattices at the theoretical limit of stiffness and strength," *Nat. Commun.* **11**(1), 1579 (2020).
28. A. Guell Izard, J. Bauer, C. Crook, V. Turlo, and L. Valdevit, "Ultrahigh Energy Absorption Multifunctional Spinodal Nanoarchitectures," *Small* **15**(45), 1903834 (2019).
29. A. Marino, O. Tricinci, M. Battaglini, C. Filippeschi, V. Mattoli, E. Sinibaldi, and G. Ciofani, "A 3D Real-Scale, Biomimetic, and Biohybrid Model of the Blood-Brain Barrier Fabricated through Two-Photon Lithography," *Small* **14**(6), 1702959 (2018).
30. F. Klein, B. Richter, T. Striebel, C. M. Franz, G. Von Freymann, M. Wegener, and M. Bastmeyer, "Two-component polymer scaffolds for controlled three-dimensional cell culture," *Adv. Mater.* **23**(11), 1341–1345 (2011).
31. A. Marino, C. Filippeschi, G. G. Genchi, V. Mattoli, B. Mazzolai, and G. Ciofani, "The Osteoprint: A bioinspired two-photon polymerized 3-D structure for the enhancement of bone-like cell differentiation," *Acta Biomater.* **10**(10), 4304–4313 (2014).
32. P. F. Jacobs, *Rapid Prototyping and Manufacturing: Fundamentals of Stereolithography* (McGraw-Hill, Inc., 1993).
33. R. Wang, K. J. Cheng, R. C. Advincula, and Q. Chen, "On the thermal processing and mechanical properties of 3D-printed polyether ether ketone," *MRS Commun.* **9**(3), 1046–1052 (2019).
34. D. Wu, Z. Zhao, Q. Zhang, H. J. Qi, and D. Fang, "Mechanics of shape distortion of DLP 3D printed structures during UV post-curing," *Soft Matter* **15**(30), 6151–6159 (2019).

35. J. S. Oakdale, J. Ye, W. L. Smith, and J. Biener, "Post-print UV curing method for improving the mechanical properties of prototypes derived from two-photon lithography," *Opt. Express* **24**(24), 27077–27086 (2016).
36. C. K. Ober, "Materials systems for 2-photon lithography," in *Three-Dimensional Microfabrication Using Two-Photon Polymerization* (Elsevier, 2020), pp. 143–174
37. Nanoscribe GmbH, *Photonic Professional (GT) User Manual* (2017).
38. Nanoscribe GmbH, *Material Safety Data Sheet: IP-Dip Photoresist* (2017).
39. ASTM International, *Standard Test Method for Compressive Properties of Rigid Plastics* (2008), i, pp. 1–8.
40. ASTM International, *Standard Test Method for Tensile Properties of Plastics* (2003), 08, pp. 46–58.
41. A. Ovsianikov, X. Shizhou, M. Farsari, M. Vamvakaki, C. Fotakis, and B. N. Chichkov, "Shrinkage of microstructures produced by two-photon polymerization of Zr-based hybrid photosensitive materials," *Opt. Express* **17**(4), 2143 (2009).
42. J. T. Fourkas, "Fundamentals of Two-Photon Fabrication," in *Three-Dimensional Microfabrication Using Two-Photon Polymerization*, Tommaso Baldacchini, ed. (William Andrew Publishing, 2016), pp. 45–61.
43. J. B. Mueller, J. Fischer, Y. J. Mange, T. Nann, and M. Wegener, "In-situ local temperature measurement during three-dimensional direct laser writing," *Appl. Phys. Lett.* **103**(12), 123107 (2013).
44. C. Decker and K. Moussa, "Radical trapping in photopolymerized acrylic networks," *J. Polym. Sci., Part A: Polym. Chem.* **25**(2), 739–742 (1987).
45. M. Wen and A. V. McCormick, "A Kinetic Model for Radical Trapping in Photopolymerization of Multifunctional Monomers," *Macromolecules* **33**(25), 9247–9254 (2000).
46. C. Quan, M. Soroush, M. C. Grady, J. E. Hansen, and W. J. Simonsick, "High-temperature homopolymerization of ethyl acrylate and n-butyl acrylate: Polymer characterization," *Macromolecules* **38**(18), 7619–7628 (2005).
47. M. C. Grady, W. J. Simonsick, and R. A. Hutchinson, "Studies of higher temperature polymerization of n-butyl methacrylate and n-butyl acrylate," *Macromol. Symp.* **182**(1), 149–168 (2002).
48. S. Srinivasan and A. M. Rappe, "Theoretical Insights Into Thermal Self-Initiation Reactions of Acrylates," in *Computational Quantum Chemistry* (Elsevier, 2019), pp. 99–134.
49. A. Schroer, J. Bauer, R. Schwaiger, and O. Kraft, "Optimizing the mechanical properties of polymer resists for strong and light-weight micro-truss structures," *Extreme Mech. Lett.* **8**, 283–291 (2016).